

## Texture Analysis Methods – A Review

Andrzej Materka and Michal Strzelecki  
Technical University of Lodz, Institute of Electronics  
ul. Stefanowskiego 18, 90-924 Lodz, Poland  
tel. +48 (42) 636 0065, fax +48 (42) 636 2238

Email: [materka,mstrzel@ck-sg.p.lodz.pl](mailto:materka,mstrzel@ck-sg.p.lodz.pl), Internet: <http://www.eletel.p.lodz.pl>

**Abstract.** Methods for digital-image texture analysis are reviewed based on available literature and research work either carried out or supervised by the authors. The review has been prepared on request of Dr Richard Lerski, Chairman of the Management Committee of the COST B11 action “Quantitation of Magnetic Resonance Image Texture”.

### 1. Introduction

Although there is no strict definition of the image texture, it is easily perceived by humans and is believed to be a rich source of visual information – about the nature and three-dimensional shape of physical objects. Generally speaking, textures are complex visual patterns composed of entities, or subpatterns, that have characteristic brightness, colour, slope, size, etc. Thus texture can be regarded as a similarity grouping in an image (Rosenfeld 1982). The local subpattern properties give rise to the perceived lightness, uniformity, density, roughness, regularity, linearity, frequency, phase, directionality, coarseness, randomness, fineness, smoothness, granulation, etc., of the texture as a whole (Levine 1985). For a large collection of examples of textures see (Brodatz 1966). There are four major issues in texture analysis:

- 1) Feature extraction: to compute a characteristic of a digital image able to numerically describe its texture properties;
- 2) Texture discrimination: to partition a textured image into regions, each corresponding to a perceptually homogeneous texture (leads to image segmentation);
- 3) Texture classification: to determine to which of a finite number of physically defined classes (such as normal and abnormal tissue) a homogeneous texture region belongs;
- 4) Shape from texture: to reconstruct 3D surface geometry from texture information.

Feature extraction is the first stage of image texture analysis. Results obtained from this stage are used for texture discrimination, texture classification or object shape determination. This review is confined mainly to feature extraction and texture discrimination techniques. Most common texture models will be shortly discussed as well.

## 2. Texture analysis

Approaches to texture analysis are usually categorised into

- structural,
- statistical,
- model-based and
- transform

methods. **Structural** approaches (Haralick 1979, Levine 1985) represent texture by well-defined primitives (*microtexture*) and a hierarchy of spatial arrangements (*macrotexture*) of those primitives. To describe the texture, one must define the primitives and the placement rules. The choice of a primitive (from a set of primitives) and the probability of the chosen primitive to be placed at a particular location can be a function of location or the primitives near the location. The advantage of the structural approach is that it provides a good symbolic description of the image; however, this feature is more useful for synthesis than analysis tasks. The abstract descriptions can be ill defined for natural textures because of the variability of both micro- and macrostructure and no clear distinction between them. A powerful tool for structural texture analysis is provided by mathematical morphology (Serra 1982, Chen 1994). It may prove to be useful for bone image analysis, e.g. for the detection of changes in bone microstructure.

In contrast to structural methods, **statistical** approaches do not attempt to understand explicitly the hierarchical structure of the texture. Instead, they represent the texture indirectly by the non-deterministic properties that govern the distributions and relationships between the grey levels of an image. Methods based on second-order statistics (i.e. statistics given by pairs of pixels) have been shown to achieve higher discrimination rates than the power spectrum (transform-based) and structural methods (Weszka 1976). Human texture discrimination in terms of texture statistical properties is investigated in (Julesz 1975). Accordingly, the textures in grey-level images are discriminated spontaneously only if they differ in second order moments. Equal second-order moments, but different third-order moments require deliberate cognitive effort. This may be an indication that also for automatic processing, statistics up to the second order may be most important (Niemann 1981). The most popular second-order statistical features for texture analysis are derived from the so-called co-occurrence matrix (Haralick 1979). They were demonstrated to feature a potential for effective texture discrimination in biomedical-images (Lerski 1993, Strzelecki 1995). The approach based on multidimensional co-occurrence matrices was recently shown to outperform wavelet packets (a transform-based technique) when applied to texture classification (Valkealathi 1998).

**Model based** texture analysis (Cross 1983, Pentland 1984, Chellappa 1985, Derin 1987, Manjunath 1991, Strzelecki 1997), using fractal and stochastic models, attempt to interpret an image texture by use of, respectively, generative image model and stochastic model. The parameters of the model are estimated and then used for image analysis. In practice, the computational complexity arising in the estimation of stochastic model parameters is the primary problem. The fractal model has been shown to be useful for modelling some natural textures. It can be used also for texture analysis and

discrimination (Pentland 1984, Chaudhuri 1995, Kaplan 1995, Cichy 1997); however, it lacks orientation selectivity and is not suitable for describing local image structures.

**Transform methods** of texture analysis, such as Fourier (Rosenfeld 1980), Gabor (Daugman 1985, Bovik 1990) and wavelet transforms (Mallat 1989, Laine 1993, Lu 1997) represent an image in a space whose co-ordinate system has an interpretation that is closely related to the characteristics of a texture (such as frequency or size). Methods based on the Fourier transform perform poorly in practice, due to its lack of spatial localisation. Gabor filters provide means for better spatial localisation; however, their usefulness is limited in practice because there is usually no single filter resolution at which one can localise a spatial structure in natural textures. Compared with the Gabor transform, the wavelet transforms feature several advantages:

- varying the spatial resolution allows it to represent textures at the most suitable scale,
- there is a wide range of choices for the wavelet function, so one is able to choose wavelets best suited for texture analysis in a specific application.

They make the wavelet transform attractive for texture segmentation. The problem with wavelet transform is that it is not translation-invariant (Brady 1996, Li 1997).

### 3. Models of texture

Features (parameters) derived from AR model, Gaussian-Markov RMF model and the Gibbs RMF (Derin 1987) are used for image segmentation.

#### 3.1 AR models

The autoregressive (AR) model assumes a local interaction between image pixels in that pixel intensity is a weighted sum of neighbouring pixel intensities. Assuming image  $f$  is a zero-mean random field, an AR causal model can be defined as

$$f_s = \sum_{r \in N_s} \theta_r f_r + e_s \quad (3.1)$$

where  $f_s$  is image intensity at site  $s$ ,  $e_s$  denotes an independent and identically distributed (i.i.d.) noise,  $N_s$  is a neighbourhood of  $s$  and  $\theta$  is a vector of model parameters. Causal AR models have an advantage of simplicity and efficiency in parameter estimation over other, non-causal spatial interaction models. Causal AR model parameters were used in (Hu 1994) for unsupervised texture segmentation. An example of a local neighbourhood for such a model, represented by 4 parameters, is shown in Fig. 3.1. Shaded area in Fig. 3 indicates region where valid causal half-plane AR model neighbourhood may be located.

Using the AR model for image segmentation consists in identifying the model parameters for a given image region and then using the obtained parameter values for texture discrimination. In the case of simple pixel neighbourhood shown in Fig. 3, that comprises 4 immediate pixel neighbours, there are 5 unknown model parameters – the standard

deviation  $\sigma$  of the driving noise  $\mathbf{e}_s$  and the model parameter vector  $\boldsymbol{\theta}=[\theta_1, \theta_2, \theta_3, \theta_4]$ . By minimising the sum of squared error

$$\sum_s e_s^2 = \sum_s (f_s - \boldsymbol{\theta} \mathbf{w}_s)^2 \quad (3.2)$$

the parameters can be estimated through the following equations:

$$\boldsymbol{\theta} = \left( \sum_s \mathbf{w}_s \mathbf{w}_s^T \right)^{-1} \left( \sum_s \mathbf{w}_s f_s \right) \quad (3.3)$$

$$\sigma^2 = N^{-2} \sum_s (f_s - \boldsymbol{\theta} \mathbf{w}_s)^2 \quad (3.4)$$

where  $\mathbf{w}_s = \text{col}[\mathbf{f}_i, i \in N_s]$ , and the square  $N \times N$  image is assumed.

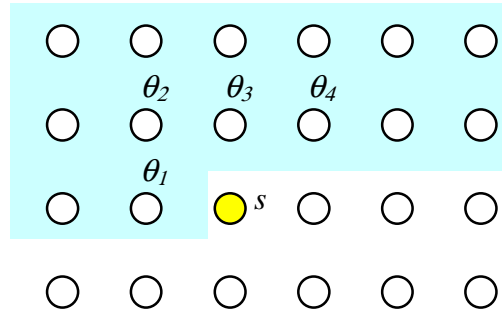


Fig. 3.1 Local neighbourhood of image element  $\mathbf{f}_s$

Recursively identified AR model parameters were used in (Sukissian 1994) for texture segmentation by means of an ANN classifier. Sarkar et al. (Sarkar 1997) considered the problem of selecting the AR model order for texture segmentation.

An extensive discussion of other stochastic models, including non-causal AR model, moving average (MA) model and the autoregressive moving average (ARMA) representation can be found in (Jain 1989).

### 3.2 Markov random fields

A Markov random field (MRF) is a probabilistic process in which all interactions is local; the probability that a cell is in a given state is entirely determined by probabilities for states of neighbouring cells (Blake 1987). Direct interaction occurs only between immediate neighbours. However, global effects can still occur as a result of propagation.

The link between the image energy and probability is that

$$p \propto \exp(-E/T) \quad (3.1)$$

where  $T$  is a constant. The lower the energy of a particular image (that was generated by a particular MRF), the more likely it is to occur.

There is a potential advantage in hidden Markov models (HMM) over other texture discrimination methods is that an HMM attempts to discern an underlying fundamental structure of an image that may not be directly observable. Experiments of texture discrimination using identified HMM parameters are described in (Povlow 1995), showing better performance than the autocorrelation method which required much larger neighbourhood, on both synthetic and real-world textures.

Another conventional approach segments statistical texture image by maximising the a posteriori probability based on the Markov random field (MRF) and Gaussian random field models (Geman 1984). Since a conditional probability density function (pdf) is not accurately estimated by the MRF, equivalently the maximum a posteriori (MAP) estimator uses the Gibbs random field. However, the Gibbs parameters are not known a priori, thus they should be estimated first for texture segmentation (Hassner 1981).

An efficient GMRF parameter estimation method, based on the histogramming technique of (Derin 1987) is elaborated in (Gurelli 1994). It does not require maximisation of a log-likelihood function; instead, it involves simple histogramming, a look-up table operation and a computation of a pseudo-inverse of a matrix with reasonable dimensions.

The least-square method for estimating the second-order MRF parameters is used in (Yin 1994) for unsupervised texture segmentation by means of a Kohonen artificial neural network.

In (Yin 1994), MRF and Kohonen ANN were used for unsupervised texture segmentation, while genetic algorithms have been applied in (Andrey 1998).

Using the MRF for colour texture segmentation was introduced in (Panjwani 1995). A maximum pseudolikelihood scheme was elaborated for estimation model parameters from texture regions. The final stage of the segmentation algorithm is a merging process that maximises the conditional likelihood of an image. The problem of selecting neighbours during the design of colour RMF is still to be investigated. Its importance is justified by the fact that large number of parameters that can be used to define interactions within and between colour bands may increase the complexity of the approach. Colour texture MRF models are considered in (Bennett 1998).

The problem of texture discrimination using Markov random fields and small samples is investigated in (Speis 1996). The analysis revealed that  $20 \times 20$  samples contain enough information to distinguish between textures and that the poor performance of MRF reported before should be attributed to the fact that Markov fields do not provide accurate models for textured images of many real surfaces.

Multiresolution approach to using GMRF for texture segmentation appears more effective compared to single resolution analysis (Krishnamachari 1997). Parameters of lower resolution are estimated from the fine resolution parameters. The coarsest

resolution data are first segmented and the segmentation results are propagated upward to the finer resolution.

### 3.3 Fractal models

There is an observation that the fractal dimension (FD) is relatively insensitive to an image scaling (Pentland 1984) and shows strong correlation with human judgement of surface roughness. It has been shown that some natural textures have a linear log power spectrum, and that the processing in the human visual system (i.e. the Gabor-type representation) is well suited to characterise such textures. In this sense, the fractal dimension is an approximate spectral estimator, comparable to other alternative methods (Chaudhuri 1995).

Fractal models describe objects that have high degree of irregularity. Statistical model for fractals is fractional Brownian motion (C-C. Chen 1989, Peitgen 1992, Jennane 1994). The 2D fractional Brownian motion (fBm) model provides a useful tool to model textured surfaces whose roughness is scale-invariant. The average power spectrum of an fBm model follows a  $1/f$  law; it is characterised by the self-similarity condition

$$\text{var}[f(t+s) - f(t)] = \sigma^2 |s|^{2H} \quad (3.2)$$

where  $0 < H < 1$  is known as the Hurst parameter (a one-dimensional process is considered, for simplicity). The self-similarity condition is stationary in the sense that the power law is independent of the time parameter  $t$ . The major disadvantage of fBm is that the appearance of its realisation is controlled by the single Hurst parameter  $H$ . Thus the roughness of the realisations is invariant to scale. Another disadvantage is that the model is isotropic. The extended self similarity (ESS) model was proposed in (Kaplan 1995) to deal with these limitations, such that

$$\text{var}[f(t+s) - f(t)] = \sigma^2 g(s) \quad (3.3)$$

where  $g(1) = 1$ . The function  $g(s)$  is called the structure function, which determines the appearance of the 2D random model of a texture. It is related to the image correlation function. For the ESS model a generalised Hurst parameter is defined for isotropic images. This parameter is scale-dependent; it is calculated by taking a logarithm of a ratio of average local energy of image horizontal and vertical increments at available scales. The parameters derived can be used for texture analysis, as shown in (Kaplan 1995). Further research is needed to find the ESS model suitability to non-isotropic textures.

The fractal dimension  $D$  of a signal characterised by an fBm is equal to (Jennane 1994)

$$D = E + 1 - H \quad (3.4)$$

where  $E$  is the Euclidean dimension ( $E = 2$  for a curve,  $E = 3$  for a surface). A number of methods for calculation of image fractal dimension is described in (S. Chen 1993, Sarkar 1994).

The fractal dimension of six images derived from the original texture and the concept of multifractal model that implies a continuous spectrum of exponents were utilised in (Chaudhuri 1995) for natural texture segmentation.

The ability of fractal features to segment mosaics of natural texture images was investigated in (Duibuisson 1994). It was concluded that fractal dimensions will not segment all types of texture.

There were attempts to segment the grey and white matters and lateral ventricles in magnetic resonance (MR) images based on fractal models – as reported by (Lundhall 1986) and (Lachman 1992).

### 3.4 Other models

An interesting texture model is suggested in (Doh 1996) using the metric space concept, a special form of the topology space. Each pixel is regarded as a set element and region segmentation of texture images is modelled by the topology structure of each class. Topology is a mathematically defined relationship among elements. Closure set is the largest topology member of the set. The segmentation algorithm is based on the concept of the metric space and closure. A number of theorems are proven in (Doh 1996) that form the theoretical basis to the segmentation procedure. Computer simulation for synthesised and real texture images shows that the proposed algorithm gives better performance than the conventional Gauss-Markov random field (GRMF) and the spatial grey level difference method (SGLDM) methods.

## 4. Feature extraction techniques

### 4.1 First-order histogram based features

Assume the image is a function  $f(x,y)$  of two space variables  $x$  and  $y$ ,  $x=0,1,\dots,N-1$  and  $y=0,1,\dots,M-1$ . The function  $f(x,y)$  can take discrete values  $i = 0,1,\dots,G-1$ , where  $G$  is the total number of number of intensity levels in the image. The intensity-level histogram is a function showing (for each intensity level) the number of pixels in the whole image, which have this intensity:

$$h(i) = \sum_{x=0}^{N-1} \sum_{y=0}^{M-1} \delta(f(x,y), i) , \quad (4.1)$$

where  $\delta(j,i)$  is the Kronecker delta function

$$\delta(j,i) = \begin{cases} 1, & j = i \\ 0, & j \neq i \end{cases} . \quad (4.2)$$

The histogram of intensity levels is obviously a concise and simple summary of the statistical information contained in the image. Calculation of the grey-level histogram involves single pixels. Thus the histogram contains the first-order statistical information about the image (or its fragment). Dividing the values  $h(i)$  by the total number of pixels in the image one obtains the approximate probability density of occurrence of the intensity levels

$$p(i) = h(i)/NM, \quad i = 0, 1, \dots, G-1 \quad (4.3)$$

The histogram can be easily computed, given the image. The shape of the histogram provides many clues as to the character of the image. For example, a narrowly distributed histogram indicated the low-contrast image. A bimodal histogram often suggests that the image contained an object with a narrow intensity range against a background of differing intensity. Different useful parameters (image features) can be worked out from the histogram to quantitatively describe the first-order statistical properties of the image. Most often the so-called central moments (Papoulis 1965) are derived from it to characterise the texture (Levine 1985, Pratt 1991), as defined by Equations (4.4)-(4.7) below.

$$\text{Mean:} \quad \mu = \sum_{i=0}^{G-1} ip(i) \quad (4.4)$$

$$\text{Variance:} \quad \sigma^2 = \sum_{i=0}^{G-1} (i - \mu)^2 p(i) \quad (4.5)$$

$$\text{Skewness:} \quad \mu_3 = \sigma^{-3} \sum_{i=0}^{G-1} (i - \mu)^3 p(i) \quad (4.6)$$

$$\text{Kurtosis:} \quad \mu_4 = \sigma^{-4} \sum_{i=0}^{G-1} (i - \mu)^4 p(i) - 3 \quad (4.7)$$

Two other parameters are also used, described in (4.8) and (4.9).

$$\text{Energy:} \quad E = \sum_{i=0}^{G-1} [p(i)]^2 \quad (4.8)$$

$$\text{Entropy:} \quad H = - \sum_{i=0}^{G-1} p(i) \log_2[p(i)] \quad (4.9)$$

The mean takes the average level of intensity of the image or texture being examined, whereas the variance describes the variation of intensity around the mean. The skewness is zero if the histogram is symmetrical about the mean, and is otherwise either positive or negative depending whether it has been skewed above or below the mean. Thus  $\mu_3$  is an indication of symmetry. The kurtosis is a measure of flatness of the histogram; the



component ‘3’ inserted in (4.7) normalises  $\mu_4$  to zero for a Gaussian-shaped histogram. The entropy is a measure of histogram uniformity. Other possible features derived from the histogram are the minimum, the maximum, the range and the median value.

In the case of visual images, the mean and variance do not actually carry the information about the texture. They rather represent the image acquisition process, such as the average lighting conditions or the gain of a video amplifier. Using images normalised against both the mean and variance can give better texture discrimination accuracy than using the actual mean and the actual variance as texture parameters (Lam 1997). Thus images are often normalised to have the same mean, e.g.  $\mu = 0$ , and the same standard deviation, e.g.  $\sigma = 1$ .

Information extracted from local image histograms is used in (Lowitz 1983) as features for texture segmentation. In particular, the module and state of the histogram are suggested for quantitative texture description. For the pixel  $(x,y)$  centred in a window containing  $N$  pixels, the module is

$$I_{MH}(x, y) = \sum_{i=0}^{G-1} \frac{h(i) - N/G}{\sqrt{h(i)[1 - p(i)] + N/G(1 - 1/G)}} \quad (4.10)$$

It is argued in (Lowitz 1983) that the module (4.10) is a measure of information included in the histogram. The state is the intensity level that corresponds to a maximum value of intensity counts in the histogram.

## 4.2 Co-occurrence matrix based features

The major advantage of using the texture attributes (4.4)-(4.9) is obviously their simplicity. However, they can not completely characterise texture. Julesz found through his famous experiments on human visual perception of texture (Julesz 1975), that for a large class of textures “no texture pair can be discriminated if they agree in their second-order statistics”. Even if counterexamples have been found to this conjecture, the importance of the second-order statistics is certain. Therefore the major statistical method used in texture analysis is the one based on the definition of the joint probability distributions of **pairs of pixels**.

The second-order histogram is defined as the co-occurrence matrix  $h_{d\theta}(i,j)$  (Haralick 1979). When divided by the total number of neighbouring pixels  $R(d,\theta)$  in the image, this matrix becomes the estimate of the joint probability,  $p_{d\theta}(i,j)$ , of two pixels, a distance  $d$  apart along a given direction  $\theta$  having particular (co-occurring) values  $i$  and  $j$ . Two forms of co-occurrence matrix exist – one symmetric where pairs separated by  $d$  and  $-d$  for a given direction  $\theta$  are counted, and other not symmetric where only pairs separated by distance  $d$  are counted. Formally, given the image  $f(x,y)$  with a set of  $G$  discrete intensity levels, the matrix  $h_{d\theta}(i,j)$  is defined such that its  $(i,j)$ th entry is equal to the number of times that

$$f(x_1, y_1) = i \text{ and } f(x_2, y_2) = j \quad (4.11)$$

where

$$(x_2, y_2) = (x_1, y_1) + (d \cos \theta, d \sin \theta) \quad (4.12)$$

This yields a square matrix of dimension equal to the number of intensity levels in the image, for each distance  $d$  and orientation  $\theta$ . Due to the intensive nature of computations involved, often only the distances  $d = 1$  and 2 pixels with angles  $\theta = 0^\circ, 45^\circ, 90^\circ$  and  $135^\circ$  are considered as suggested in (Haralick 1979). If pixel pairs in the image are highly correlated, the entries in  $h_{d\theta}(i, j)$  will be clustered along the diagonal of the matrix. Co-occurrence matrix calculation is illustrated in Fig. 1, for  $d = 1$ . The classification of fine textures requires small values of  $d$ , whereas coarse textures require large values of  $d$ . Reduction of the number of intensity levels (by quantizing the image to fewer levels of intensity) helps increase the speed of computation, with some loss of textural information.

0	0	1	1
0	0	1	1
0	2	2	2
2	2	3	3

Image example

$i \setminus j$	0	1	2	3
0	#(0,0)	#(0,1)	#(0,2)	#(0,3)
1	#(1,0)	#(1,1)	#(1,2)	#(1,3)
2	#(2,0)	#(2,1)	#(2,2)	#(2,3)
3	#(3,0)	#(3,1)	#(3,2)	#(3,3)

Construction of co-occurrence matrix

4	2	1	0
2	4	0	0
1	0	6	1
0	0	1	2

$h_{1,0^\circ}$

6	0	2	0
0	4	2	0
2	2	2	2
0	0	2	0

$h_{1,90^\circ}$

Fig. 4.1 The spatial co-occurrence calculations (Haralick 1979)

The co-occurrence matrix contains  $G^2$  elements that is too much for texture analysis in a reasonable time. A reduced number of features can be calculated using the co-occurrence matrix for the purpose of texture discrimination in (Haralick 1979, Pratt 1991). Some of them are defined by the equations that follow, where  $\mu_x, \mu_y$  and  $\sigma_x, \sigma_y$  denote the mean and standard deviations of the row and column sums of the matrix, respectively [related to the marginal distributions  $p_x(i)$  and  $p_y(j)$ ].

$$\text{Angular second moment (energy): } \sum_{i=0}^{G-1} \sum_{j=0}^{G-1} [p(i, j)]^2 \quad (4.13)$$

$$\text{Correlation: } \sum_{i=0}^{G-1} \sum_{j=0}^{G-1} \frac{ijp(i, j) - \mu_x \mu_y}{\sigma_x \sigma_y} \quad (4.14)$$

$$\text{Inertia (contrast):} \quad \sum_{i=0}^{G-1} \sum_{j=0}^{G-1} (i-j)^2 p(i, j) \quad (4.15)$$

$$\text{Absolute value:} \quad \sum_{i=0}^{G-1} \sum_{j=0}^{G-1} |i-j| p(i, j) \quad (4.16)$$

$$\text{Inverse difference:} \quad \sum_{i=0}^{G-1} \sum_{j=0}^{G-1} \frac{p(i, j)}{1+(i-j)^2} \quad (4.17)$$

$$\text{Entropy:} \quad - \sum_{i=0}^{G-1} \sum_{j=0}^{G-1} p(i, j) \log_2 [p(i, j)] \quad (4.18)$$

$$\text{Maximum probability:} \quad \max_{i, j} p(i, j) \quad (4.19)$$

An expansion of the set of features derived from the co-occurrence matrix can be found in (Lerski 1993, Pratt 1991).

A fast algorithm for the computation of co-occurrence matrix parameters was proposed in (Alparone 1990, Argenti 1990). A generalised multidimensional co-occurrence matrices are considered in (Kovalev 1996) that exploit the co-occurrence of not only grey levels at some distance and directions, but also such features as e.g. magnitude of local Sobel gradient. The authors called this approach “elementary structure balance method”.

An increase in the co-occurrence dimensionality, which improves the description of spatial relationships, benefits both monochrome and colour texture segmentation (Valkealathi 1998).

### 4.3 Multiscale features

For calculating multiscale features, various time-frequency methods are adopted (L. Cohen 1989). The most commonly used are Wigner distributions, Gabor functions, and wavelet transforms. However, Wigner distributions are found to possess interference terms between different components of a signal. These interference terms lead to wrong signal interpretation. Gabor filters are criticised for their non-orthogonality that results in redundant features at different scales or channels (Teuner 1995). Still, Gabor filters are used for texture segmentation (P. Cohen 1989, Jain 1991, Dunn 1994, Bigun 1994) and the problem of designing Gabor filters for texture segmentation is considered in (Dunn 1995, Teuner 1995). On the other hand, the wavelet transform, being a linear operation, does not produce interference terms. Unlike the Fourier transform, it possesses a capability of time (space) localisation of signal spectral features. For these reasons, much interest in applications of the wavelet transform to texture analysis can be noticed recently. Dyadic wavelet transform is considered here.

The wavelet decomposition of a signal  $f(x)$  is performed by a convolution of the signal with a family of basis functions,  $\psi_{2^s, t}(x)$ :

$$\langle f(x), \psi_{2^s, t}(x) \rangle = \int_{-\infty}^{\infty} f(x) \psi_{2^s, t}(x) dx \quad (4.20)$$

where  $s, t$  are referred to as the translation and dilation parameters, respectively.

A pyramidal algorithm (Mallat 1989) can perform wavelet decomposition in which a pair of wavelet filters including a lowpass filter and a highpass filter is utilised to calculate wavelet coefficients (4.20). The quadrature mirror filters (QMF) as depicted in Fig. 4.2 can be used to implement wavelet transform instead of explicitly using wavelet functions (Strang 1996).

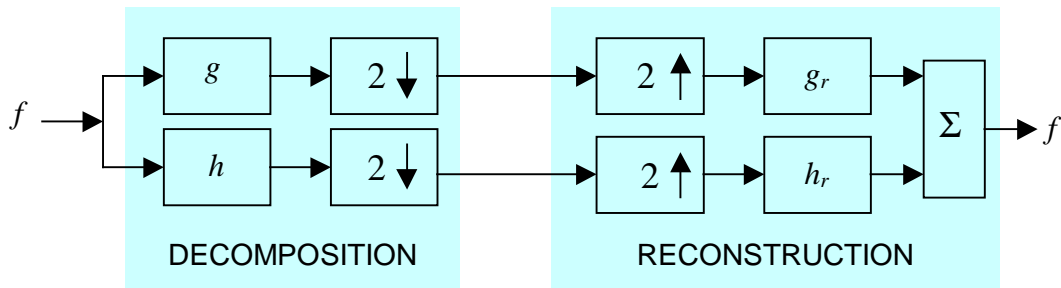


Fig. 4.2 Illustration of wavelet-based signal decomposition and reconstruction  
 $g, g_r$  – lowpass filters;  $h, h_r$  – highpass filters;  
 $(2\downarrow)$  – downsampling (decimation by 2);  $(2\uparrow)$  – upsampling.

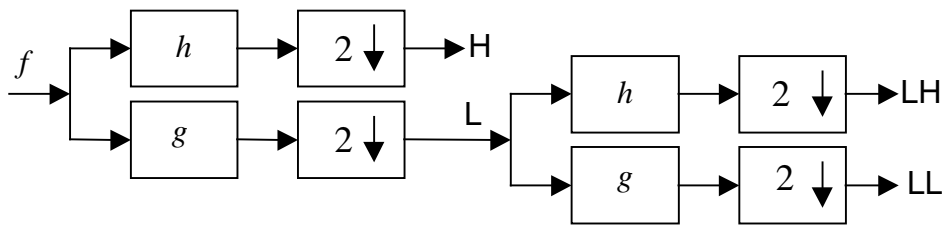


Fig. 4.3 Signal analysis using 2 levels of dyadic wavelet decomposition  
L – approximation components, H – detail components

In the case of two-dimensional images, the wavelet decomposition is obtained with separable filtering along the rows and along the columns of an image (Mallat 1989). Fig. 4.4 illustrates the level 1 (1-scale) and level 2 (2-scale) image decomposition.

The wavelet analysis can thus be interpreted as image decomposition in a set of independent, spatially oriented frequency channels. The HH subimage represents diagonal details (high frequencies in both directions – the corners), HL gives horizontal high frequencies (vertical edges), LH gives vertical high frequencies (horizontal edges), and the image LL corresponds to the lowest frequencies. At the subsequent scale of analysis, the image LL undergoes the decomposition using the same  $g$  and  $h$  filters, having always the

lowest frequency component located in the upper left corner of the image. Each stage of the analysis produces next 4 subimages whose size is reduced twice compared to the previous scale. Good texture segmentation results can be obtained within 2 to 4 scales of wavelet decomposition. In the case of a 3-scale analysis, 10 frequency channels can be identified as shown in Fig. 4.5. The size of the wavelet representation is the same as the size of the original image. As there is a choice of particular wavelet function for image analysis, symmetric wavelet functions appear superior to non-symmetric ones (Lu 1997) which is attributed to the linear-phase property of symmetric filters.

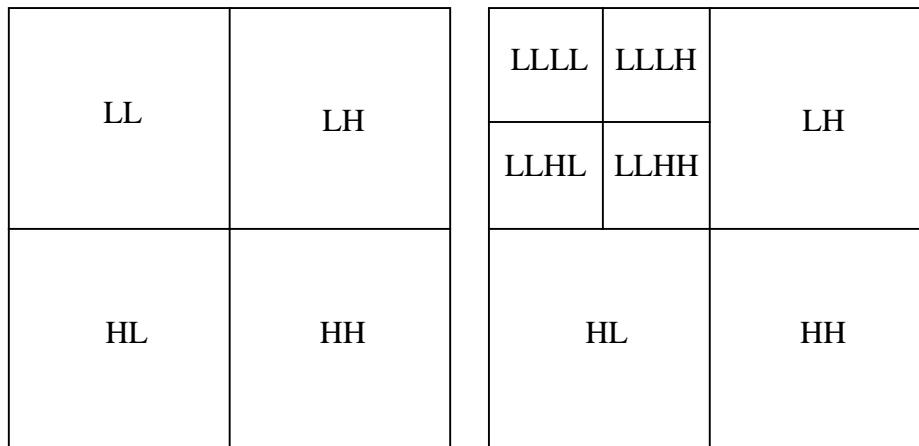


Fig. 4.4 One-scale decomposition (left), two-scale decomposition (right)

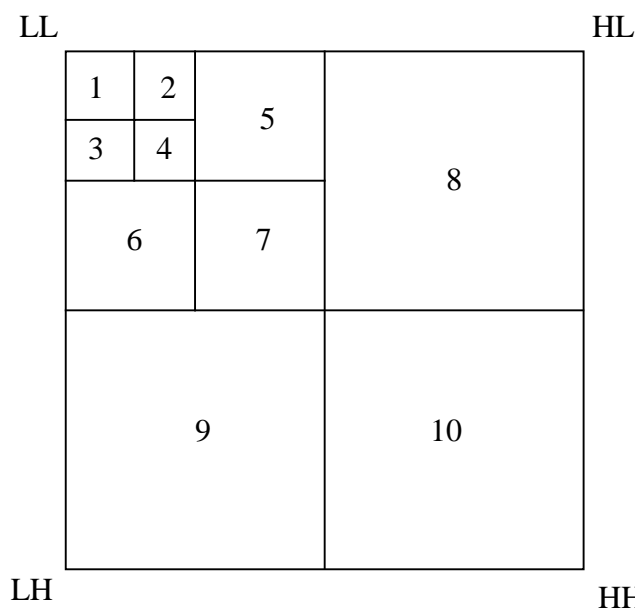


Fig. 4.5 Ten channels of a three-level wavelet decomposition of an image

In (Porter 1996) wavelet transform is used both to analyse the image prior to segmentation enabling feature selection as well as to provide spatial frequency-based descriptors for segmenting textures. The quality and accuracy of segmentation ultimately depend on the type of features used. Images consisting of a number of textured regions are best segmented using frequency-based features, whereas images made up of smoother regions can more easily be segmented using local mean and variance of intensity levels.

Different features are required in different regions of the image. Three-level wavelet decomposition was used in (Porter 1996), resulting in 10 main wavelet channels. The “energy” of each channel can be evaluated by simply calculating the mean magnitude of its wavelet coefficients.

$$C_n = \frac{1}{MN} \sum_{x=0}^{M-1} \sum_{y=0}^{N-1} |w(x,y)| \quad (4.21)$$

where the channel is of dimensions  $M$  by  $N$  (usually  $M = N$ ) and  $w$  is a wavelet coefficient within a channel. It turns out that textured images have large energies in both low and middle frequencies. The low-frequency channels are dominant over smooth regions.

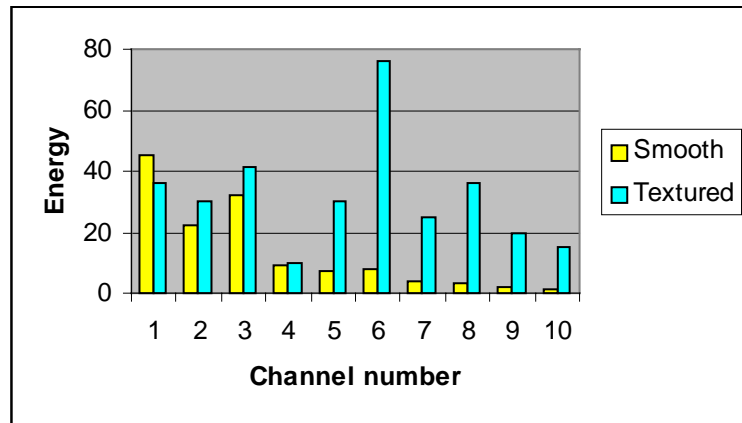


Fig. 4.6 Example energy levels for smooth and textured images

To decide what kind of features to use for image segmentation, the image is first split into smooth and textured regions based on the value of the following factor

$$R = \frac{C_1 + C_2 + C_3 + C_4}{C_5 + C_6 + C_7} \quad (4.22)$$

The region is labelled as smooth if  $R \geq T$  or textured if  $R < T$ , where  $T$  is the threshold. Appropriate features are then selected for the regions, to perform the segmentation as illustrated in Fig. 4.7.

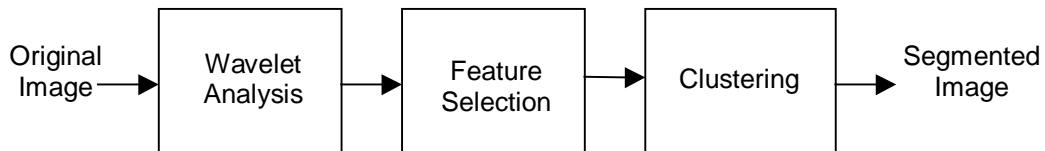


Fig. 4.7 Block diagram of the segmentation algorithm (Porter 1996)

#### 4.4 Other features

A Grey-Tone Difference Matrix (GTDM) was suggested in (Amadasun 1989) in an attempt to define texture measures correlated with human perception of textures. A GTD matrix is a column vector containing  $G$  elements. Its entries are computed based on

measuring the difference between the intensity level of a pixel and the average intensity computed over a square, sliding window centred at the pixel. Suppose the image intensity level  $f(\mathbf{x}, \mathbf{y})$  at location  $(\mathbf{x}, \mathbf{y})$  is  $i$ ,  $i=0, 1, \dots, G-1$ . The average intensity over a window centred at  $(\mathbf{x}, \mathbf{y})$  is

$$\bar{f}_i = \bar{f}(x, y) = \frac{1}{W-1} \sum_{m=-K}^K \sum_{n=-K}^K f(x+m, y+n) \quad (4.20)$$

where  $K$  specifies the window size and  $W = (2K+1)^2$ . The  $i$ -th entry of the gray-tone difference matrix is

$$s(i) = \sum_{x=0}^{M-1} \sum_{y=0}^{N-1} |i - \bar{f}_i| \quad (4.21)$$

for all pixels having the intensity level  $i$ . Otherwise,  $s(i) = 0$ .

Five different features were derived from the GTDM, to quantitatively describe such perceptual texture properties as

- coarseness (defined by the size of texture primitives):

$$C_{\text{cos}} = \left( \varepsilon + \sum_{i=0}^{G-1} p_i s(i) \right)^{-1} \quad (4.22)$$

where  $\varepsilon$  is a small number to prevent the coarseness coefficient becoming infinite and  $p_i$  is the estimated probability of the occurrence of the intensity level  $i$

$$p_i = N_i / n \quad (4.23)$$

with  $N_i$  denoting the number of pixels that have the level  $i$ , and  $n = (N-K)(M-K)$ .

- contrast (dependent on the intensity difference between neighbouring pixels):

$$C_{\text{con}} = \left[ \frac{1}{N_t(N_t - 1)} \sum_{i=0}^{G-1} \sum_{j=0}^{G-1} p_i p_j (i - j)^2 \right] \left[ \frac{1}{n} \sum_{i=0}^G s(i) \right] \quad (4.24)$$

- busyness (described by high spatial frequency of intensity changes):

$$C_{\text{bus}} = \frac{\sum_{i=0}^{G-1} p_i s(i)}{\sum_{i=0}^{G-1} \sum_{j=0}^{G-1} |ip_i - jp_j|}, \quad p_i \neq 0, p_j \neq 0 \quad (4.25)$$

- complexity (dependent on the number of different primitives and different average intensities):

$$C_{\text{com}} = \sum_{i=0}^{G-1} \sum_{j=0}^{G-1} \frac{|i-j|}{n(p_i + p_j)} [p_i s(i) + p_j s(j)], \quad p_i \neq 0, p_j \neq 0 \quad (4.26)$$

- texture strength (clearly definable and visible primitives):

$$C_{str} = \frac{\sum_{i=0}^{G-1} \sum_{j=0}^{G-1} (p_i + p_j)(i - j)^2}{\varepsilon + \sum_{i=0}^{G-1} s(i)}, \quad p_i \neq 0, p_j \neq 0 \quad (4.27)$$

The original paper (Amadasun 1989) contains more detailed explanation about the reasoning that led to the particular definition of texture features given by Equations (4.22)-(4.27).

Examples of commonly used features, not discussed above, are

- Fourier transform energy,
- local extrema count along a 1D scan direction (Mitchell 1977),
- run length matrix-derived features (Haralick 1979),
- directional intensity level energy (Hsiao 1989),
- filter masks in the space domain (multichannel filtering, Law features) including Gabor filters (P. Cohen 1989, Jain 1991, Dunn 1994, Bigun 1994) and subsequent nonlinear operators (Cohen 1990, Jain 1996),
- filter masks in the Fourier spectrum domain (Delibasis 1997),
- mathematical morphology-derived features (Chen 1994, Lam 1997),
- statistical geometrical features (Y. Chen 1995: 16 features that describe geometry of binary images obtained from texture by multithresholding).

#### 4.5 Feature selection

- (Fukunaga 1990): Choosing most effective features for class separability (different to the criteria for image representation).
- (Lerski 1993): Strongly skewed features are rejected; strongly correlated features are rejected. Discriminatory analysis is used to select the most discriminating features (an analysis of variance F-test was applied).
- (Kovalev 1996): The most desirable line of approach is to pay a lot of attention in choosing image features so that the classes are linearly separable. In other words, careful feature selection followed by a simple classifier is much more preferable than a quick feature selection stage followed by a carefully designed classifier.

### 5. Texture discrimination and segmentation

The reported segmentation methods are based on:

- region growing (Pratt 1991, Gonzalez 1992),
- estimation theory – maximum likelihood (Chellappa 1985),
- split-and-merge (Chen 1979, Pratt 1991, Gonzalez 1992),
- Bayesian classification (Hsiao 1989),
- probabilistic relaxation – iterative approach for using context information to reduce local ambiguities (Hsiao 1989),
- clustering (Hu 1994),
- artificial neural networks (Jain 1991, Sukissian 1994, Yin 1994, Augusteijn 1995, Strzelecki 1995, Jain 1996, Bruzzone 1998).



The techniques for texture segmentation can be classified to be either **supervised** (Hsiao 1989a, Unser 1990, Reed 1990, Bovik 1990, Dunn 1994, Dunn 1995) or **unsupervised** (Hsiao 1989b, Jain 1991, Mao 1992, Bigun 1994, Hu 1994, Yin 1994, Chaudhuri 1995, J. Chen 1995, Panjwani 1995, Kervrann 1995, Teuner 1995, Andrey 1998) based on whether the number of textures contained in the image is known in advance or not.

The most recent contributions are shortly characterised below, as they may put some light on current trends in the field.

The  $k$ -means clustering technique was used in (Porter 1996), applied to wavelet derived features. The technique involves grouping those pixels in the image whose feature vectors represent points that are close together in the feature space. The final result is a number of clusters  $K$ , where each hopefully depicts a perceptually different region in the image.

Feedforward ANNs were used in (Jain 1996) along with multichannel filtering for texture segmentation. A backpropagation algorithm was applied for the classifier training.

Improvements to iterative morphological decomposition were proposed in (Lam 1997) for rotation-invariant texture discrimination, based on features derived using mathematical morphology. The method is compared to simultaneous autoregressive (SAR) models and multichannel Gabor filters.

A comparison is presented in (Porter 1997) between the performance of three schemes of feature extraction: the wavelet transform, a circularly symmetric Gabor filter and a GMRF with a circular neighbour set to achieve rotation-invariant texture discrimination. In conclusion, the wavelet-based approach was the most accurate, exhibited the best noise performance and had the lowest computational complexity when implemented using the db4 wavelet.

Experiments with natural textures were performed in (Valkealathi 1998) using reduced multidimensional co-occurrence histograms. They proposed linear compression, dimension optimisation and vector quantization for the reduction of histograms. As a result, higher classification accuracy was obtained compared to the channel histograms and wavelet packets.

The problem always encountered in textured image segmentation relates to the trade-off between the sample size and accuracy. The bigger the sample size, the better the accuracy of feature estimation; however, this allows a coarse segmentation only. Image segmentation at small sample size is tackled in (Speis 1996) where RMF was used as image model. Boundary effect (a pixel at texture boundary has neighbouring pixels belonging to different textures) is investigated in (Yhann 1995) where multiresolution method was combined with detecting local intensity discontinuities at the boundary.

## 6. MRI Texture Classification

A limited number of recently published contributions is quoted here, as a result of the early stage of this literature survey. *[(?) denotes a situation in which original papers were not accessible to the authors at the time of completing the manuscript of this survey.]*

- (Lundhall 1986): Segmentation of grey and white matter and lateral ventricles using a fractal model (?).
- (Lachmann 1992): Fractal model (?).
- (Bello 1994): Combination of wavelet analysis and multiresolution MRF. First, discrete wave-packet transform is used to focus on selected image “channel” data. Second, an MRF segmentation is used to “fuse” data associated with the selected image channels at a specific resolution levels. Applied to brain image segmentation to distinguish “empty space”, “white matter”, “grey matter”, “internal brain cavities” and “neck/muscle/skin”. Qualitative characteristics of the derived segmentation described as “good”.
- (Delibasis 1997): Genetic algorithm-designed filter masks correlated with image Fourier spectrum. Segmentation of cerebellum from MR images.
- (Bruzzone 1998): Magnetic resonance images supervised classification using so-called structural neural networks shows more accuracy than a k-NN classifier. Images were first segmented using a region-growing algorithm. Each region was represented by a feature vector (features related to intensity, position and size-and-shape) to excite the SNN. Twelve classes were associated with different organs (e.g. the nose, the left eye, the brain, etc.).

## 7. Work carried out at the Institute of Electronics, TUL

A number of different methods concerning texture analysis and synthesis has been developed in the Institute of Electronics since 1990. For purposes of texture analysis and segmentation statistical methods using co-occurrence matrix, micro-feature extraction and Markov random field models were implemented. Among these methods, the multilayer perceptron (MLP) network and the cellular neural network (CNN) were utilised. Texture synthesis methods were based on the CNN approach.

### 7.1 Co-occurrence matrix method

This statistical approach, which is based on co-occurrence matrices (Haralick 1979) describes second-order statistics of texture. An algorithm for co-occurrence matrix construction and statistical feature extraction from the matrix may be defined as follows:

- a) Division of analysed image into connected and disjoint regions. An image is considered as a set of points distributed on two-dimensional and finite space. Intensities of image points are integer values from range  $[0, \dots, G-1]$  where  $G$  is the number of intensity levels.
- b) Construction of co-occurrence matrix  $H$  for each region and some vectors  $\mathbf{v}$ , where  $H[i,j]$  is a matrix of estimated probabilities of transitions from level  $i$  to level  $j$  for

given vector  $\mathbf{v}$  where  $i, j = 0, 1, \dots, G-1$ , and vector  $\mathbf{v}$  defines direction of construction of  $H$  and distance between points that have intensities  $i$  and  $j$ .

- c) Computation of  $R$  statistical features considered as representative for a given class of texture, derived from matrix  $H$ .
- d) Classification of textures using a classifier with  $R$  inputs and  $K$  outputs, where  $K$  is number of classes.

As a classifier, the multilayer perceptron (MLP) artificial neural network was used for textured image segmentation in (Strzelecki 1995). The single-hidden layer architecture of the MLP is illustrated in Fig. 7.1. The texture features are fed to the network inputs. The layer of hidden processing elements links the network input and output. The number of output neurons is set according to the number of texture classes. The index of an output neuron that shows a maximum activation level indicates the texture class that corresponds to actual ANN input. Thanks to the non-linear activation function  $f_s$  of the network elements, the MLP can form arbitrary complex decision boundaries in the classified feature space.

MLP is trained with the supervised learning algorithm known as the backpropagation of the gradient of the error, i.e. the difference (defined usually by the minimum mean square value criterion) between the actual and desired network output (Hecht-Nielsen 1990). Computational cost of the training stage heavily depends on the number of neurons in the network. Also, more importantly, the number of neurons determines network classification capabilities.

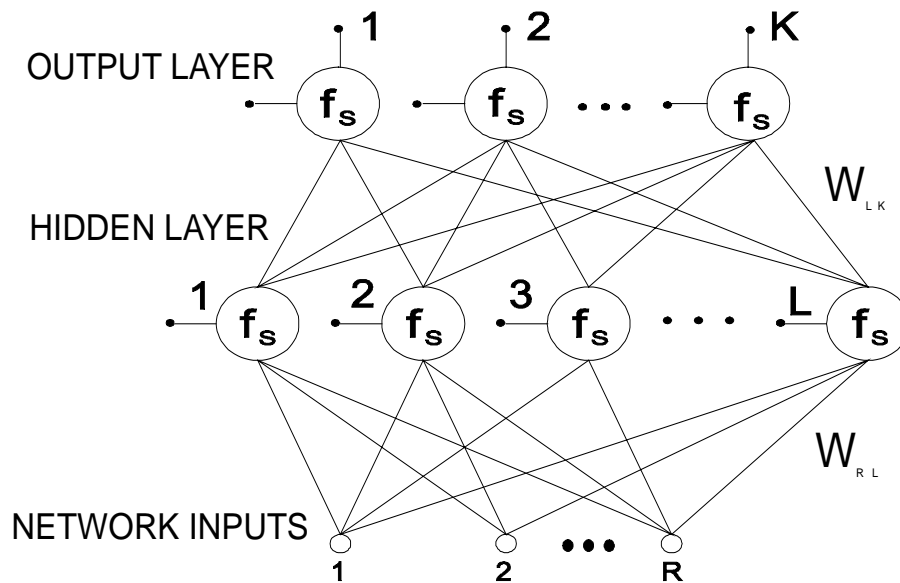


Fig. 7.1 MLP artificial neural network ( $f_s$  denotes the nonlinear activation function)

The choice of the number and the type of statistical features computed using the co-occurrence matrixes was made based on multidimensional variance analysis, which provides optimal set of features for given segmentation task.

Examples of texture segmentation using the co-occurrence matrix method are presented in Fig. 7.2a and 7.2b. They represent cross-section of human skin tissue: epidermis – region marked with ‘1’, dermis (‘2’) and the mast cells (‘3’). The problem was to find the area occupied by the mast cells that is important in diagnosis of some kinds of skin cancers (for example *urticaria pigmentosa*). Both pictures are represented as arrays of 512x512 pixels with 128 intensity levels.

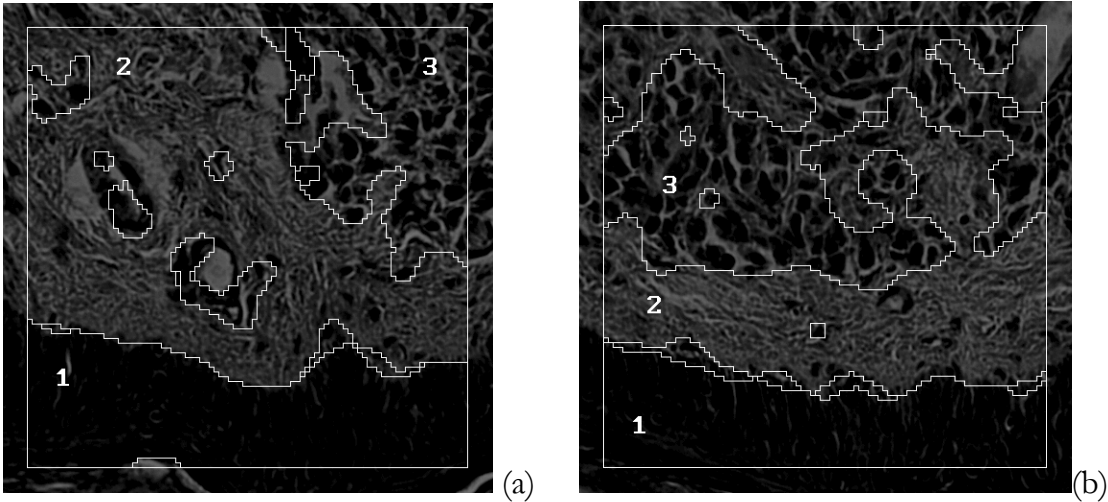


Fig. 7.2 Skin tissues after segmentation

The image shown in Fig. 7.3 presents mast cells and their position with respect to dermoepidermal junction. The CM method was used to find this junction. The measured distance of mast cells to this junction is one of important characteristics of mast cells morphology.

The aim of this study was to elaborate a texture analysis method that would allow describing morphology and localisation of mast cells in the skin. This research was performed with collaboration of Department of Dermatology, Medical University of Lodz.

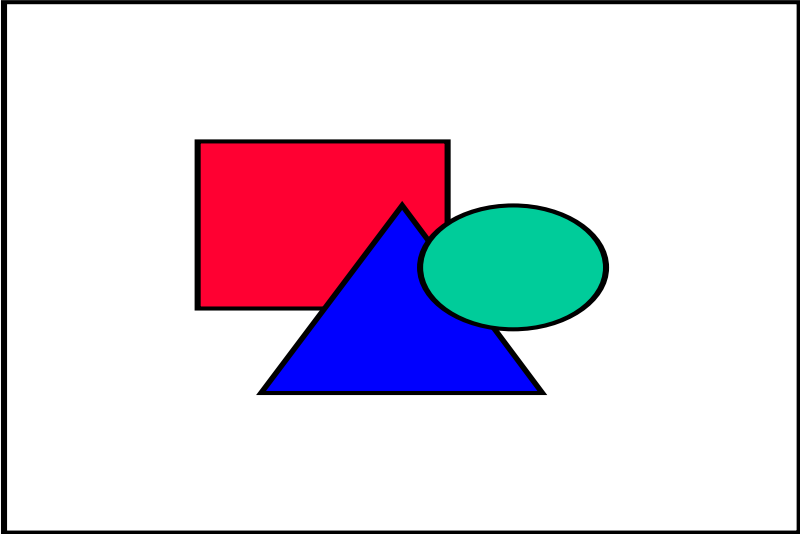


Fig. 7.3 Mast cells (white) and the dermoepidermal junction (staircase line)

## 7.2 Texture segmentation based on micro-feature extraction

In this approach the texture is assumed to contain random/periodic transitions of image brightness, called *micro-features* (Pelczynski 1994), e.g. edges, line segments or set of points which have specific spatial intensity distribution. These local features can be extracted by performing two-dimensional convolution of an image with a particular filter mask that represents a model of the micro-feature pattern. Then, if required, a further nonlinear transformation of the image obtained after the convolution may be performed. Examples of  $3 \times 3$  masks used for local feature detection are illustrated in Fig. 7.4.

-1	0	-1
0	4	0
-1	0	-1

a)

-1	0	1
-2	0	2
-1	0	1

b)

-1	2	-1
-2	4	-2
-1	2	-1

c)

Fig. 7.4 Examples of micro-feature detection masks: a) point detector, b) vertical edge detector, c) vertical line-like structure detector

As in the co-occurrence matrix method, the calculated feature values are fed to MLP network, which is used as a classifier. An example of segmentation of sample biomedical image is presented in Fig. 7.5.

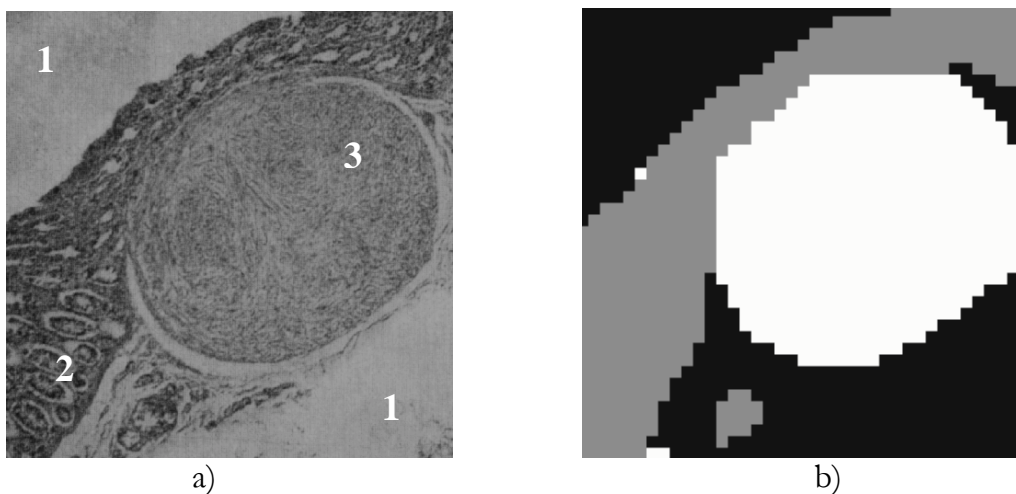


Fig. 7.5 Segmentation of sample microscopic image representing biological tissues: a) source image with three texture classes, b) image after segmentation.

In the next approach, a cellular neural network (CNN) was used both for texture feature extraction and texture segmentation. CNNs is an array of nonlinear filters with local feedback connections that enhance their filtering capabilities. A single CNN table is a two-dimensional array composed of identical computational elements, or cells (Figs. 7.6 and 7.7). Each element has input and is locally connected with other cells in the network. Weights between all inputs and the element, from its **neighbourhood**, form the so-called weight **template**. The weight template is identical for every element in a network. Fig. 7.8 illustrates the proposed network structure for texture classification.

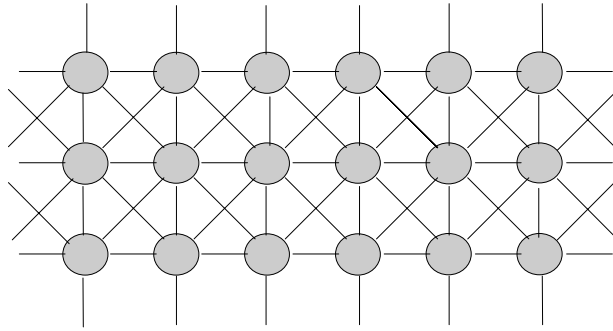


Fig. 7.6 An array of cellular neural network cells of neighbourhood 1

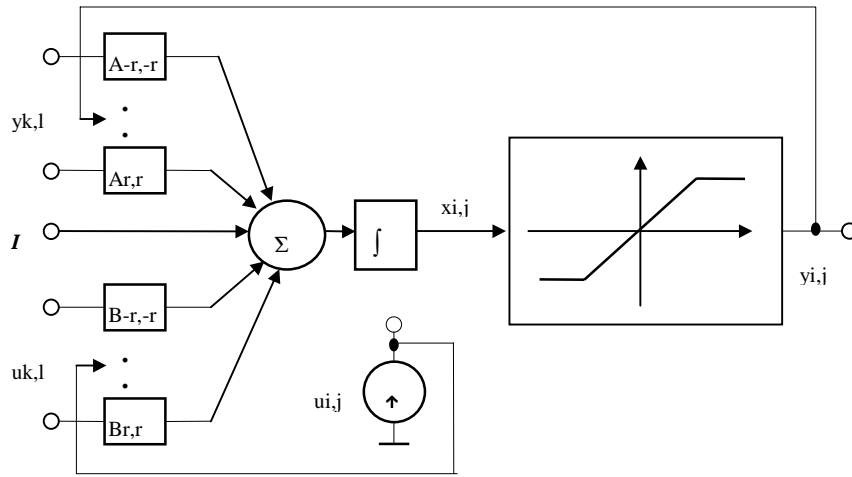


Fig. 7.7 Block diagram of a single CNN cell

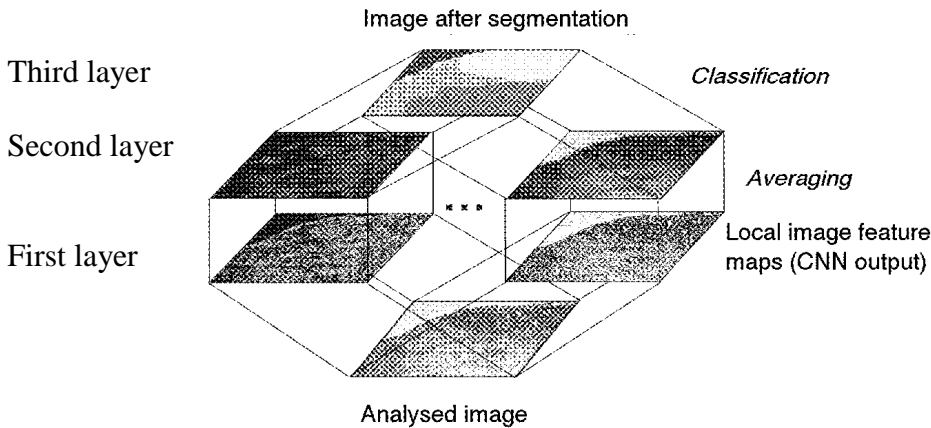


Fig. 7.8 Cellular neural network architecture for texture segmentation

First layer of the network consists of CNN tables, each associated with one class of recognisable texture. Each of these CNN tables detects local features of only one texture and remains insensitive to others. Second network layer performs linear averaging of the first layer outputs, providing statistical measure of detected local texture features. Intensities of considered feature maps serve as inputs to the classification layer. In the experiments, a very simple classification rule was implemented which assumed that the highest output of feature map indicates proper texture class. Two-dimensional array of

such classifiers can form the third network layer. This structure performs fully parallel texture segmentation process. In case of hardware network realisation it provides real-time image segmentation. For template elements setting, genetic algorithm was used (Pelczynski 1997).

The proposed CNN model for texture segmentation was tested on images derived from the Brodatz album. An example of segmentation results is shown in Fig. 7.9.

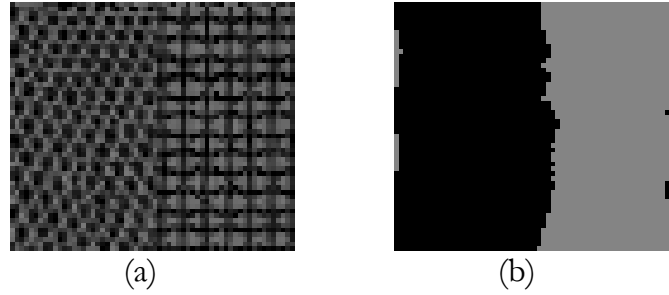


Fig. 7.9 Example of texture classification using CNN  
a) original image, b) image after segmentation

### 7.3 Markov random field model

In this method, an alternative approach to texture representation is presented. The texture is assumed as a realisation of a Markov random field. MRFs have proved to be good models for some classes of textures. Parameters of MRF uniquely describe a modelled texture and can be derived directly from the analysed image, provided MRF is an adequate model (Geman 1984, Derin 1987).

Assume  $F[\mathbf{x}, \mathbf{y}]$  is an image array of size  $N \times M$  and  $f[\mathbf{x}, \mathbf{y}]$  denotes the integer intensity level value in the range of  $[0, G-1]$  at location  $(\mathbf{x}, \mathbf{y})$ .  $F[\mathbf{x}, \mathbf{y}]$  is an MRF realisation if:

$$p(f[x, y] | f[u, v], u = 1, \dots, x-1, x+1, \dots, N, v = 1, \dots, y-1, y+1, \dots, M) = p(f[x, y] | f[u, v], (u, v) \in Q) \quad (7.1)$$

where  $p(\cdot)$  denotes conditional probability of  $f[\mathbf{x}, \mathbf{y}]$  for a given field realisation  $F[\mathbf{x}, \mathbf{y}]$  and  $Q$  denotes a neighbour set. As an example, the conditional probability for pixel  $f[\mathbf{x}, \mathbf{y}]$  in the case of a second-order four-intensity-level MRF is given by

$$p(f[x, y] | Q) = \frac{e^{-V(Q, \mathbf{a}_f, \mathbf{b})}}{\sum_{k=0}^{G-1} e^{-V(Q, \mathbf{a}_k, \mathbf{b})}} \quad (7.2)$$

where  $k$  is the intensity level,  $\mathbf{a}=[a_0, a_1, \dots, a_3]$  is color parameter vector,  $\mathbf{b}=[b_1, b_2, b_3, b_4]$  is spatial-dependency parameter vector,  $Q$  is a neighborhood of pixel  $f[i, j]$ ,  $V$  is the potential function (Derin 1987), that depends on pixel intensity  $f$  and vectors  $\mathbf{a}$  and  $\mathbf{b}$ .

Assuming that the analysed texture can be described by the MRF model, there is a need for estimating the field parameters, i.e. the vectors  $\mathbf{a}$  and  $\mathbf{b}$ . For this purpose, the likelihood maximisation method (Cross 1983), histogramming method or modified histogramming method can be used (Derin 1987). Likelihood maximisation method

provides high estimation accuracy but requires long computation time. The histogramming method is fast but less accurate, especially when used for estimation of spatial-dependency vector parameter **b**. The modified histogramming method is a combination of likelihood maximisation and histogramming, where estimation of MRF parameters is performed independently for vectors **a** and **b** (Strzelecki 1997).

As an example of texture modelling using MRFs let us consider an image shown in Fig. 7.10a that represents cross-section of striated muscle tissue. This four-intensity-level image of size 128×128 pixels was assumed as being a third-order MRFs realisation. For comparison, two estimation methods were used to obtain MRF parameter set: maximum likelihood and modified histogramming method. Next, using the obtained two sets of MRF parameters for image from Fig. 7.10a, two textures were synthesised assuming the same MRF order. They were generated using the so-called Gibbs sampler (Geman 1984). These synthetic textures are presented in Fig. 7.10b and 7.10c, respectively. As can be observed, they are very similar to the real tissue picture, which proves usefulness of the MRF to modelling the particular biomedical texture considered. The ability of modified histogramming method for providing accurate MRF parameter estimation is also demonstrated.

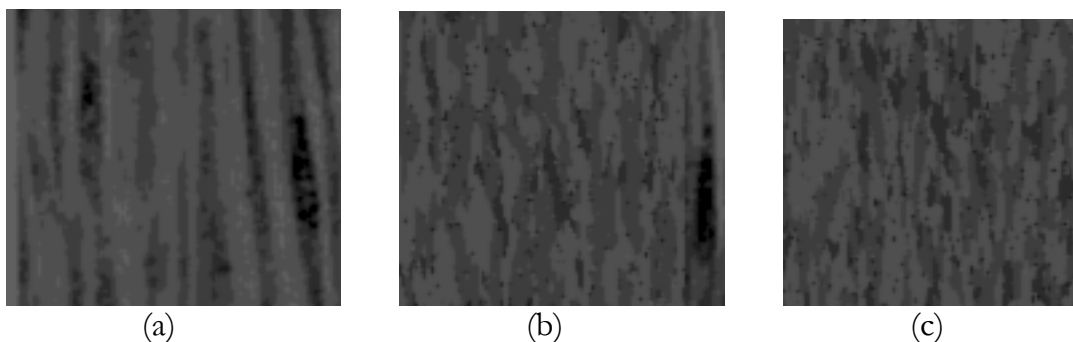


Fig. 7.10 Cross-section of striated muscle tissue (a). Textures synthesised on the basis of parameters estimated for the image of Fig. 7.10a using maximum likelihood method (b) and modified histogramming method (c)

#### **7.4 Design of cellular neural networks for texture generation**

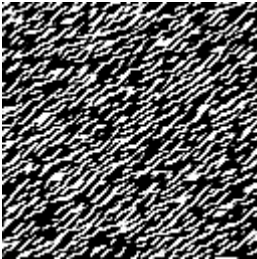
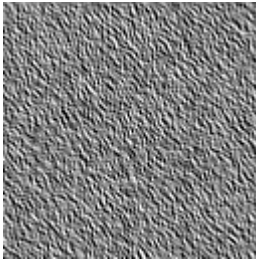
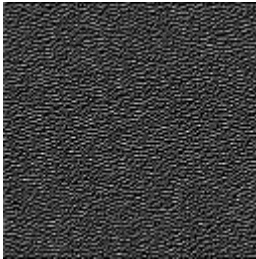
The objective of this research is to work out the texture generation method using the cellular neural network (CNN) concept (Debiec 1998). The possibility of VLSI realisation of CNN provides a powerful and efficient tool for texture synthesis that is very important in computer graphics as well as in telecommunication data compression systems. The reason for including this work in the present review on texture analysis methods is the expectation that the template identified for a given texture can be used as a feature matrix for texture discrimination as well, which will be the subject of further research.

CNN requires proper template design, whose element values are responsible for adequate network functioning. To design a network template required for texture synthesis, two methods are used. One of them uses a genetic algorithm. The search for optimal template



requires modification of network template population, which elements were randomly generated. The template is designed based on minimisation of chosen fitness function. The generation procedure starts from white noise image with small variance. This initial image is processed by the CNN for each template from its population. Next, for the texture image obtained at the network outputs, the values of statistical features are calculated and compared with values required. The ‘best fitted’ templates are chosen as parent templates for the next populations, which are created using reproduction, crossover and mutation. These operations work on binary strings used for coding of template element values. The learning procedure is stopped when the fitness function value reaches a given value.

**Table 1. Examples of CNN-generated textures for different number of statistical features used for their description**

		
Texture 1	Texture 2:	Texture 3:
$\mathbf{A} = \begin{matrix} 2.41 & -2.25 & -1.03 \\ -0.20 & 3.12 & 3.17 \\ -0.96 & 2.83 & 0.18 \end{matrix}$	$\mathbf{A} = \begin{matrix} 0.39 & -0.08 & 0.33 \\ -1.13 & -0.19 & 1.47 \\ 0.54 & 1.73 & -2.63 \end{matrix}$	$\mathbf{A} = \begin{matrix} 0.22 & -2.07 & 0.81 \\ 2.94 & 0.20 & -2.75 \\ -2.30 & -0.18 & 0.18 \end{matrix}$
Feature value: required      obtained VAR = 0.85   VAR = 0.85	Feature values: required      obtained VAR = 0.50   VAR = 0.55 EX = 0.00   EX = 0.00	Feature values: required      obtained VAR <sub>x</sub> = 0.20   VAR <sub>x</sub> = 0.33 VAR <sub>y</sub> = 0.40   VAR <sub>y</sub> = 0.38 EX = -0.42   EX = -0.30

( $\mathbf{A}$  – template matrix, VAR – variance, EX – expected value, VAR<sub>x</sub>, VAR<sub>y</sub> – variances of marginal distributions)

Experimental results are presented in Table 1. Texture representation using one feature only (for example variance) provides good results in terms of CNN template obtained. The texture generated using this template has the variance value the same, as it was required. Unfortunately, the increase of texture features causes less accurate results, increasing computational time significantly.

The obtained textures are very simple and they look binary. For grey-level texture generation, the alternative method was used. In this method, the CNN used for texture generation emulates an autoregressive FIR filter. To provide network stability, the initial image (white noise) and generated texture image are transformed such that they possess negative amplitude spectrum and phase spectrum equal to zero. The objective of template design process is to obtain a stable CNN that generates a texture with the same amplitude spectrum as an original image (in terms of mean-square error).

Using this method, the CNN were designed for generation of some Brodatz textures (t09\_gras, t04\_cork, t93\_furc, and t104\_bur). The results are presented in Fig. 7.11 and 7.12. It can be stated that the proposed method provides good results for the stochastic textures. For deterministic textures, such as t104\_bur, phase spectrum equal to zero causes substantial reconstruction errors. Thus the problem under investigation is to find methods appropriate for phase spectrum modelling.

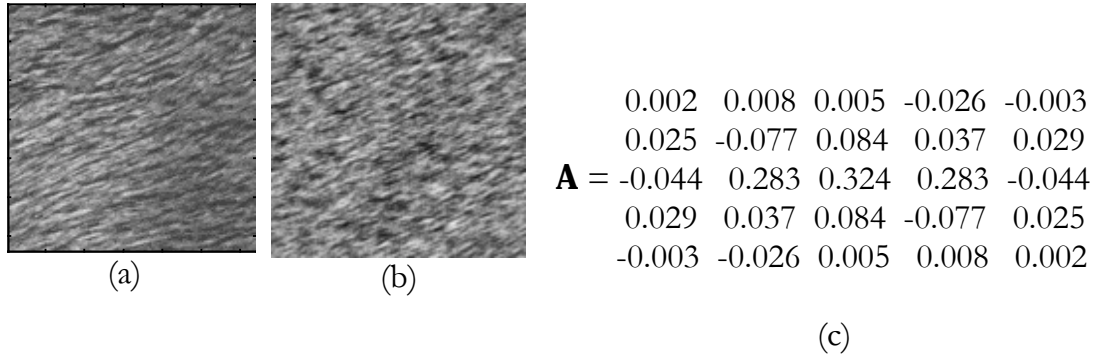


Fig. 7.11 Original texture t93\_furc (a)  
synthesised texture (b) the corresponding CNN template  $\mathbf{A}$  (c)

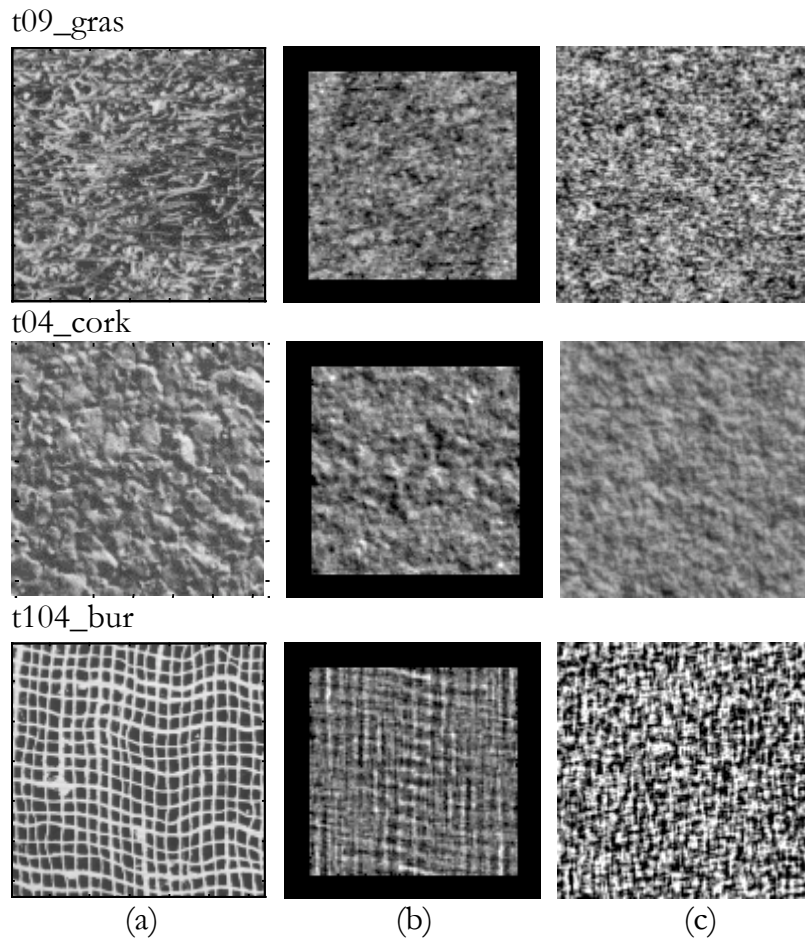


Fig. 7.12 Original textures (a), texture fragments with zero phase spectrum (b),  
synthesised textures using the CNN (c)

## 7.4 Radiographic texture analysis

Image analysis techniques for detection of changes in bone mineral density (BMD) are examined in (Cichy 1997). The results are compared with BMD measured using dual-energy X-ray absorptiometry (DXA) method. X-ray patterns were registered in the same conditions of exposure and chemical development. Additionally, a calibration phantom was used to standardise the results. Radiogram patterns were digitised with a CCD camera. The following texture parameters were computed: the mean of intensity, standard deviation of intensity, skewness, kurtosis, energy, entropy and fractal dimension. The mean value, standard deviation and coefficient of linear correlation with BMD were estimated for every parameter. Occurrence probability of intensity level is highly correlated with DXA-measured results. It seems that analysis of fractal dimension can additionally enrich diagnostic knowledge about bone microarchitecture. Examples of bone tissue X-ray images are presented in Fig. 13.

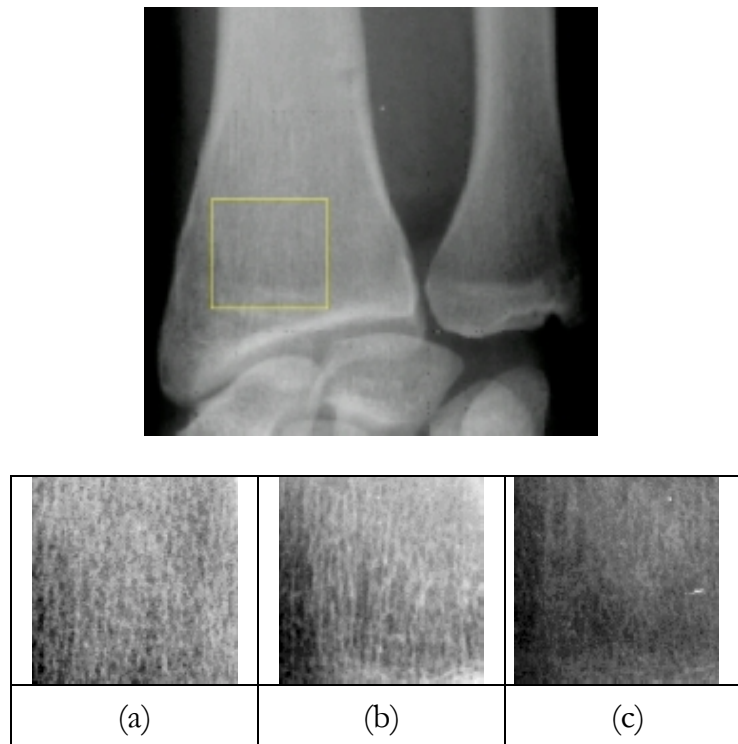


Fig. 7.13 Sample X-ray images of bone tissue for different BMD coefficients  
(a) - BMD=0.56, (b) - BMD=0.31, (c) - BMD=0.14.

## 8. Summary

The above review of texture analysis methods is by no means exhaustive. Further library search and numerical investigation are needed to make the material collected more complete. Investigation of actual MR image properties would make the search for adequate texture analysis methods better focused.

## Acknowledgment

The authors wish to thank Mr Piotr Cichy, Mr Piotr Debiec and Mr Pawel Pelczynski for providing figures included in Chapter 7, respectively Fig. 13; Figs 6, 7, 11, 12; and Figs 4, 5, 8, 9.

## References

### 1965

A. Papoulis, *Probability, Random Variables and Stochastic Processes*, McGraw-Hill, 1965.

### 1966

P. Brodatz, *Textures - A Photographic Album for Artists and Designers*, Dover, 1966.

### 1975

B. Julesz, "Experiments in the Visual Perception of Texture", *Scientific American*, **232**, 4, 1975, 34-43.

### 1976

J. Weszka, C. Dey and A. Rosenfeld, "A Comparative Study of Texture Measures for Terrain Classification", *IEEE Trans. System, Man and Cybernetics*, **6**, 269-285, 1976.

### 1977

O. Mitchell, C. Myers and W. Boyne, "A Max-Min Measure for Image Texture Analysis", *IEEE Trans. Computers*, 408-414, 1977.

### 1979

R. Haralick, "Statistical and Structural Approaches to Texture", *Proc. IEEE*, **67**, 5, 786-804, 1979.

P. Chen and T. Pavlidis, "Segmentation by Texture Using a Co-Occurrence Matrix and a Split-and Merge Algorithm", *CGIP*, **10**, 1979, 172-182.

### 1980

A. Rosenfeld and J. Weszka, "Picture Recognition" in *Digital Pattern Recognition*, K. Fu (Ed.), Springer-Verlag, 135-166, 1980.

### 1981

M. Hassner and J. Sklansky, "The Use of Markov Random Fields as Models of Texture", *Image Modelling* A. Rosenfeld (Ed.), Academic Press, 1981, 185-198.

H. Niemann, *Pattern Analysis*, Springer-Verlag, 1981.

### 1982

A. Rosenfeld and A. Kak, *Digital Picture Processing* vol. 1, Academic Press, 1982.

J. Serra, *Image Analysis and Mathematical Morphology*, Academic Press, 1982.

### 1983

G. Cross and A. Jain, "Markov Random Field Texture Models", *IEEE Trans. Pattern Analysis and Machine Intelligence*, **5**, 1, 25-39, 1983.

G. Lowitz, "Can a Local Histogram Really Map Texture Information?", *Pattern Recognition*, **16**, 2, 1983, 141-147.

### 1984

S. Geman and D. Geman, "Stochastic Relaxation, Gibbs Distribution and the Bayesian Restoration of Images", *IEEE Trans. Pattern Analysis and Machine Intelligence*, **6**, 11, 1984, 721-741.

A. Pentland, "Fractal-Based Description of Natural Scenes", *IEEE Trans. Pattern Analysis and Machine Intelligence*, **6**, 6, 661-674, 1984.

### 1985

R. Chellappa and S. Chatterjee, "Classification of Textures Using Gaussian Markov Random Fields", *IEEE Trans. Acoustic, Speech and Signal Processing* **33**, 4, 959-963, 1985.

J. Daugman, "Uncertainty Relation for Resolution in Space, Spatial Frequency and Orientation Optimised by Two-Dimensional Visual Cortical Filters", *Journal of the Optical Society of America*, **2**, 1160-1169, 1985.

M. Levine, *Vision in Man and Machine*, McGraw-Hill, 1985.

### 1987

A. Blake and A. Zisserman, *Visual Reconstruction*, The MIT Press, 1987.

H. Derin and H. Elliot, "Modeling and Segmentation of Noisy and Textured Images Using Gibbs Random Fields", *IEEE Trans. Pattern Analysis and Machine Intelligence*, **9**, 1, 39-55, 1987.

### 1989

M. Amadasun and R. King, "Textural Features Corresponding to Textural Properties", *IEEE Transactions on System, Man Cybernetics*, **19**, 5, 1989, 1264-1274.

C-C. Chen, J. Daponte and M. Fox, "Fractal Feature Analysis and Classification in Medical Imaging", *IEEE Trans. Medical Imaging* **8**, 2, 1990, 133-142.

L. Cohen, "Time-Frequency Distributions – A Review", *Proceedings IEEE*, **77**, 7, 1989, 941-981.

P. Cohen, C. LeDinh and V. Lacasse, "Classification of Natural Textures by Means of Two-Dimensional Orthogonal Masks", *IEEE Trans. Acoustics, Speech and Signal Processing* **37**, 1, 1989, 125-128.

J. Hsiao and A. Sawchuk, "Supervised Textured Image Segmentation Using Feature Smoothing and Probabilistic Relaxation Techniques", *IEEE Trans. Pattern Analysis and Machine Intelligence*, **11**, 12, 1989, 1279-1292.

J. Hsiao and A. Sawchuk, "Supervised Textured Image Segmentation Using Feature Smoothing and Probabilistic Relaxation Techniques", *CVGIP*, **48**, 1989, 1-20.

A. Jain, *Fundamentals of Digital Image Processing* Prentice Hall, 1989.

S. Mallat, "Multifrequency Channel Decomposition of Images and Wavelet Models", *IEEE Trans. Acoustic, Speech and Signal Processing* **37**, 12, 1989, 2091-2110.

## 1990

- L. Alparone, F. Argenti and G. Benelli, "Fast Calculation of Co-Occurrence Matrix Parameters For Image Segmentation", *Electronics Letters*, **26**, 1, 1990, 23-24.
- F. Argenti, L. Alparone and G. Benelli, "Fast Algorithms for Texture Analysis Using Co-Occurrence Matrices", *IEE Proceedings*, **137**, F, 6, 1990, 443-448.
- A. Bovik, M. Clark and W. Giesler, "Multichannel Texture Analysis Using Localised Spatial Filters", *IEEE Trans. Pattern Analysis and Machine Intelligence*, **12**, 1990, 55-73.
- K. Fukunaga, *Introduction to Statistical Pattern Recognition*, Academic Press, 1990
- R. Hecht-Nielsen, *Neurocomputing* Addison-Wesley, 1990.
- T. Reed and H. Wechsler, "Segmentation of Textured Images and Gestalt Organization Using Spatial/Spatial-Frequency Representations", *IEEE Trans. Pattern Analysis and Machine Intelligence*, **12**, 1, 1990, 1-12.
- M. Unser and M. Eden, "Nonlinear Operators for Improving Texture Segmentation Based on Features Extracted by Spatial Filtering", *IEEE Trans. System Man Cybernetics*, **20**, 4, 1990, 804-815.

## 1991

- F. Cohen, Z. Fan and M. Patel, "Classification of Rotated and Scaled Textured Images Using Gaussian Markov Random Field Models", *IEEE Trans. Pattern Analysis and Machine Intelligence*, **13**, 2, 192-202, 1991.
- A. Jain and F. Farrokhnia, "Unsupervised Texture Segmentation Using Gabor Filters", *Pattern Recognition*, **24**, 12, 1991, 1167-1186.
- B. Manjunath and R. Chellappa, "Unsupervised Texture Segmentation Using Markov Random Fields", *IEEE Trans. Pattern Analysis and Machine Intelligence*, **13**, 5, 478-482, 1991.
- W. Pratt, *Digital Image Processing* Wiley, 1991.

## 1992

- R. Gonzalez and R. Woods, *Digital Image Processing* Addison-Wesley, 1992.
- J. Mao and A. Jain, "Texture Classification and Segmentation Using Multiresolution Simultaneous Autoregressive Models", *Pattern Recognition*, **25**, 2, 1992, 173-188.
- H-O. Peitgen, H. Jurgens and D. Saupe, *Chaos and Fractals*, Springer-Verlag, 1992.

## 1993

- S. Chen, J. Keller and R. Crownover, "On the Calculation of Fractal Features from Images", *IEEE Trans. Pattern Analysis and Machine Intelligence*, **15**, 10, 1993, 1087-1090.
- A. Laine and J. Fan, "Texture Classification by Wavelet Packet Signatures", *IEEE Trans. Pattern Analysis and Machine Intelligence*, **15**, 11, 1993, 1186-1191.
- R. Lerski, K. Straughan, L. Shad, D. Boyce, S. Blumel, and I. Zuna, "MR Image Texture Analysis – An Approach to Tissue Characterisation", *Magnetic Resonance Imaging* **11**, 1993, 873-887.

## 1994

- M. Bello, "A Combined Markov Random Field and Wave-Packet Transform-Based Approach for Image Segmentation", *IEEE Trans. Image Processing* **3**, 6, 1994, 834-846.
- J. Bigun and J. du Buf, "N-folded Symmetries by Complex Moments in Gabor Space and Their Application to Unsupervised Texture Segmentation", *IEEE Trans. Pattern Analysis and Machine Intelligence*, **16**, 1, 1994, 80-87.

- Y. Chen and E. Dougherty, "Grey-Scale Morphological Granulometric Texture Classification", *Optical Engineering* **33**, 8, 1994, 2713-2722.
- M-P. Dubuisson and R. Dubes, "Efficacy of Fractal Features in Segmenting Images of Natural Textures", *Pattern Recognition Letters*, **15**, 1994, 419-431.
- D. Dunn, W. Higgins and J. Wakeley, "Texture Segmentation Using 2-D Gabor Elementary Functions", *IEEE Trans. Pattern Analysis and Machine Intelligence*, **16**, 2, 1994, 130-149.
- M. Gurelli and L. Onural, "On a Parameter Estimation Method for Gibbs-Markov Fields", *IEEE Trans. Pattern Analysis and Machine Intelligence*, **16**, 4, 1994, 424-430.
- Y. Hu and T. Dennis, "Textured Image Segmentation by Context Enhanced Clustering", *IEE Proc.-Visual Image and Signal Processing* **141**, 6, 1994, 413-421.
- R. Jennane and R. Harba, "Fractional Brownian Motion: A Model for Image Texture", *SIGNAL PROCESSING VII: Theories and Applications*, M. Holt et al. (Eds.), 1994, 1389-1392.
- P. Pelczynski and P. Strumillo, "Artificial Neural Network Model for Feature Extraction and Segmentation of Visual Textures", *17-th National Conf. Circuit Theory and Electronic Systems*, Wroclaw, Poland, 1994, 489-494.
- N. Sarkar and B. Chaudhuri, "An Efficient Differential Box-Counting Approach to Compute Fractal Dimension of Image", *IEEE Trans. System Man Cybernetics*, **24**, 1, 115-120.
- L. Sukissian, S. Kollias and Y. Boutalis, "Adaptive Classification of Textured Images Using Linear Prediction and Neural Networks", *Signal Processing* **36**, 1994, 209-232.
- H. Yin and N. Allinson, "Unsupervised Segmentation of textured Images Using a Hierarchical Neural Structure", *Electronics Letters*, **30**, 22, 1994, 1842-1843.

## 1995

- M. Augusteijn, "Texture Segmentation and Classification Using Neural Network Technology", *Applied Mathematics and Computer Science*, **4**, 1995, 353-370.
- B. Chaudhuri and N. Sarkar, "Texture Segmentation Using Fractal Dimension", *IEEE Trans. Pattern Analysis and Machine Intelligence*, **17**, 1, 1995, 72-77.
- J-L. Chen and A. Kundu, "Unsupervised Texture Segmentation Using Multichannel Decomposition and Hidden Markov Models", *IEEE Trans. Image Processing* **4**, 5, 1995, 603-619.
- Y-Q. Chen, M. Nixon and D. Thomas, "Statistical Geometrical Features for Texture Classification", *Pattern Recognition*, **28**, 4, 1995, 537-552.
- D. Dunn and W. Higgins, "Optimal Gabor Filters for Texture Segmentation", *IEEE Trans. Image Processing* **4**, 7, 1995, 947-964.
- L. Kaplan and C-C. Kuo, "Texture Roughness Analysis and Synthesis via Extended Self-Similar (ESS) Model", *IEEE Trans. Pattern Analysis and Machine Intelligence*, **17**, 11, 1995, 1043-1056.
- C. Kervrann and F. Heitz, "A Markov Random Field Model-Based Approach to Unsupervised Texture Segmentation Using Local and Global Spatial Statistics", *IEEE Trans. Image Processing* **4**, 6, 1995, 856-862.
- D. Panjwani and G. Healey, "Markov Random Field Models for Unsupervised Segmentation of Textured Color Images", *IEEE Trans. Pattern Analysis and Machine Intelligence*, **17**, 11, 1995, 939-954.

- B. Povlow and S. Dunn, "Texture Classification Using Noncausal Hidden Markov Models", *IEEE Trans. Pattern Analysis and Machine Intelligence*, **17**, 10, 1995, 1010-1014.
- M. Strzelecki, *Segmentation of Textured Biomedical Images Using Neural Networks*, PhD Thesis, Technical University of Łódź, Poland, 1995 (in Polish).
- A. Teuner, O. Pichler and B. Hosticks, "Unsupervised Texture Segmentation of Images Using Tuned Matched Gabor Filters", *IEEE Trans. Image Processing* **4**, 6, 1995, 863-870.
- S. Yhann and T. Young, "Boundary Localisation in Texture Segmentation", *IEEE Trans. Image Processing* **4**, 6, 1995, 849-856.

## 1996

- M. Brady and Z-Y. Xie, "Feature Selection for Texture Segmentation", in *Advances in Image Understanding*, K. Bowyer and N. Ahuja (Eds.), IEEE Computer Society Press, 1996.
- S. Doh and R-H. Pang, "Segmentation of Statistical Texture Images Using the Metric Space Theory", *Signal Processing* **53**, 1996, 27-34.
- A. Jain and K. Karu, "Learning Texture Discrimination Masks", *IEEE Trans. Pattern Analysis and Machine Intelligence*, **18**, 2, 1996, 195-205.
- V. Kovalev and M. Petrou, "Multidimensional Co-Occurrence Matrices for Object Recognition and Matching", *GMIP*, **58**, 3, 1996, 187-197.
- R. Porter and N. Canagarajah, "A Robust Automatic Clustering Scheme for Image Segmentation Using Wavelets", *IEEE Trans. Image Processing* **5**, 4, 1996, 662-665.
- A. Speis and G. Healey, "An Analytical and Experimental Study of the Performance of Markov Random Fields Applied to Textured Images Using Small Samples", *IEEE Trans. Image Processing* **5**, 3, 1996, 447-458.
- G. Strang and T. Nguyen, *Wavelets and Filter Banks*, Wellesley-Cambridge Press, 1996.

## 1997

- P. Cichy, A. Materka and J. Tuliszkiewicz, "Computerised Analysis of X-ray Images For Early Detection of Osteoporotic Changes in the Bone", *Proc. Conf. Information Technology in Medicine TIM '97*, Jaszowiec, Poland, 53-61, 1997 (in Polish).
- K. Delibasis, P. Unrill and G. Cameron, "Designing Texture Filters with Genetic Algorithms: An Application to Medical Images", *Signal Processing* **57**, 1997, 19-33.
- W-K. Lam and C-K. Li, "Rotated Texture Classification by Improved Iterative Morphological Decomposition", *IEE Proc. - Visual Image Signal Processing* **144**, 3, 1997, 171-179.
- S. Krishnamachari and R. Chellappa, "Multiresolution Gauss-Markov Random Field Models for Texture Segmentation", *IEEE Trans. Image Processing* **6**, 2, 1997, 251-267.
- C. Lu, P. Chung and C. Chen, "Unsupervised Texture Segmentation via Wavelet Transform", *Pattern Recognition*, **30**, 5, 729-742, 1997.
- P. Pelczynski, "Cellular Neural Network for Segmentation of Textured Images", *Image Processing & Communications*, **3**, No. 3-4, 1997, 3-8.
- R. Porter and N. Canagarajah, "Robust Rotation-Invariant Texture Classification: Wavelet, Gabor Filter and GMRF Based Schemes", *IEE Proc. - Visual Image Signal Processing* **144**, 3, 1997, 180-188.
- A. Sarkar, K. Sharma and R. Sonak, "A New Approach for Subset 2-D AR Model Identification for Describing Textures", *IEEE Trans. Image Processing* **6**, 3, 1997, 407-413.



M. Strzelecki and A. Materka, "Markov Random Fields as Models of Textured Biomedical Images", *Proc. 20<sup>th</sup> National Conf. Circuit Theory and Electronic Networks KTOiUE '97*, Kolobrzeg, Poland, 493-498, 1997.

### **1998**

P. Andrey and P. Tarroux, "Unsupervised Segmentation of Markov Random Field Modelled Textured Images Using Selectionists Relaxation", *IEEE Trans. Pattern Analysis and Machine Intelligence*, **20**, 3, 1998, 252-262.

J. Bennett and A. Khotanzad, "Multispectral Random Field Models for Synthesis and Analysis of Color Images", *IEEE Trans. Pattern Analysis and Machine Intelligence*, **20**, 1, 1998, 327-332.

P. Debiec, "Design of cellular neural networks for textured image synthesis", *Zeszyty Naukowe Elektronika*, **3**, 1998, pp. (in Polish).

K. Valkealathi and E. Oja, "Reduced Multidimensional Co-Occurrence Histograms in Texture Classification", *IEEE Trans. Pattern Analysis and Machine Intelligence*, **20**, 1, 1998, 90-94.

L. Bruzzone, F. Roli and S. Serpico, "Structured Neural Networks for Signal Classification", *Signal Processing* **64**, 1998, 271-290.